Colloid Polym Sci 277:403–413 (1999)

ORIGINAL CONTRIBUTION

S. Giasson
D.A. Weitz
J.N. Israelachvili

Interactions between surfactant-coated surfaces in hydrocarbon liquids containing functionalized polymer dispersant

Received: 22 September 1998
Accepted: 11 January 1999

S. Giasson (✉)
Département de Génie Chimique
Université Laval
Sainte-Foy
Québec G1K 7P4
Canada
e-mail : sgiasson@gch.ulaval.ca
Tel.: + 1-418-656-3774
Fax: + 1-418-656-5993

D.A. Weitz
Department of Physics and Astronomy
University of Pennsylvania
209 S 33rd Street
Philadelphia
PA 19104-6396, USA

J.N. Israelachvili
Department of Chemical Engineering
University of California
Santa Barbara
CA 93106, USA

Abstract The forces and viscosity between calcium benzene sulfonate surfactant-coated mica surfaces in various hydrocarbon liquids containing a polyamine-functionalized hydrocarbon polymer ($M_W \approx 8000$) have been measured using the surface forces apparatus technique. The polymer is found to adsorb to the substrate surfaces by displacing the surfactant layer, and to produce forces that are monotonically repulsive. The forces have a maximum range of 50–100 nm ($>3R_H$), indicating that tails play a particularly important role in the interaction of this relatively low molecular weight polymer. The forces become steeply repulsive below about 10 nm ($\sim 0.6R_H$), at which point a "hard-wall" repulsion comes in that can sustain pressures greater than 100 atm. Thin-film viscosity measurements indicate that the far-field positions of the slipping planes Δ_H depend on the shear rate, showing that significant shear thinning/thickening effects occur within the outermost tail regions of the adsorbed layers during shear. The position of the slipping plane, or hydrodynamic layer thickness Δ_H, varies from $0.6R_H$ to $2R_H$ away from each surface (mica and surfactant-coated mica surfaces). Beyond the hydrodynamic layer the far-field fluid viscosity is the same as that of the bulk polymer solution. At separations below $D = 2\Delta_H$ the viscosity increases as each polymer layer is compressed. The static forces exhibited various time- and history-dependent effects, which further indicate that a number of different relaxation/equilibration processes are operating simultaneously in this complex multicomponent system. The results reveal that the interactions of tails of functionally adsorbed polymers play a more important role than previously thought. This is especially true in this study where the adsorbed polymers are of low molecular weight and where the tails may represent the largest fraction of interacting segments.

Key words Interaction – Polymer – Surface – Thin film – Rheology

Introduction

Knowledge of the structure and interactions of mixed polymer/surfactant colloidal systems is essential for simultaneously controlling the stability and rheological properties of colloidal dispersions such as emulsions and lubricating oils [1, 2]. The surfactant and polymer together provide stability against coagulation and control the viscosity of the fluid, the practical aim being to produce highly concentrated dispersions, or ad-packs, that remain stable yet not unmanageably viscous. This requires that the surfactant/polymer additives produce a short-range stabilizing repulsive force between the colloidal particles which overcomes the van der Waals

attraction, i.e., that the colloidal suspension is "sterically stabilized" [3, 4]. This can be done to a limited extent by coating colloidal surfaces with surfactant but the resulting "stability" is a tenuous one. Polymer additives further improve stability, especially when the molecules contain functional groups that bind to the surfaces, thereby ensuring that the short-range forces are repulsive. In this case the interaction force between two polymer-covered particles is determined by a combination of the van der Waals force between the two bulk media (particle) and the film-film (polymer-polymer) interaction. The dominant contribution to the film-film repulsive interaction comes from the confinement of the configurational entropy when polymer groups from the two surfaces meet; however, if the polymer does not adsorb, or if it has no functional group, the interaction between the colloidal particles may be attractive due to depletion or bridging forces [3, 5, 6], and the dispersion will become unstable.

On the other hand, polymers can also drastically increase the viscosity of a dispersion, thereby rendering it unmanageable for transportation, or the repulsive forces may be so long-ranged that high particle concentrations cannot be achieved. Because hydrodynamic interactions may dominate the equilibrium forces in highly concentrated systems [7], knowledge of the dynamic forces that act between polymer-bearing surfaces or particles when they are in relative motion becomes very important in determining the rheological behavior of sterically-stabilized dispersions. Dynamic techniques have been introduced for directly measuring the dynamic interactions of liquids confined in very thin films between two surfaces and for obtaining viscosity profiles (i.e., the viscosity as a function of the distance between the two surfaces) [8–10]. It has already been shown that the viscosities of films of simple molecules as thin as ten molecular diameters are well described by their bulk viscosities even at relatively high shear rates [8]. However, similar measurements of the viscosity profiles between polymer-bearing surfaces have shown that the shear viscosity increases as the film thickness falls below a few R_g, the unperturbed radius of gyration of the polymer. These studies suggested a correlation between the viscosity profile and the range of steric interactions between the polymer-covered surfaces [9].

This work describes the results of measurements of the static and dynamic interactions of a new polyamine-functionalized hydrocarbon polymer (to be referred to as the polymer dispersant or PD) adsorbed to mica and on calcium sulfonate surfactant-coated mica surfaces in various hydrocarbon solvents. The main practical aim was to characterize such systems and to determine the optimum conditions for producing high concentrations of colloids in oil without causing instability or an unacceptably high viscosity. To this end surface forces apparatus (SFA) measurements were complemented by dynamic light scattering (DLS) measurements of the size of the colloidal particles with different dispersants adsorbed on the surface, and by measurements of the viscosity as a function of film thickness and as a function of concentration of the dispersant.

Experimental

Polymer dispersants

The three PDs studied with the SFA, to be referred to as PD-I, PD-II and PD-III, contain a branched polyamine of M_W 300–350 to which are covalently attached 1–2 polyethylene-butylene (35 wt% ethylene) molecules of average M_W 3000–3900. The overall M_W of each polymer was about 7000–9000. The polymers were synthesized and provided by Exxon Chemical Company, Paramins Division, and some of their other properties are listed in Table 1.

The DLS measurements were performed using molecules of the same class, but of different sizes, as determined by the degree of polymerization, which modifies their hydrodynamic radii (this will be addressed later). The smallest of the molecules studied with DLS corresponded closely in size to those used for the SFA measurements.

Surfactant

The calcium alkylbenzene sulfonate (CaABS) surfactant, which was also supplied by Exxon Chemical Company, was the same as that used in a number of previous studies of colloidal interactions [11, 12]. The point of attachment of the 24-carbon alkyl chain to the benzene ring is random, which means that the mixture consists of single-chain and double-chain molecules. The surfactant was purified (removed from oil) as previously described by Gee and Israelachvili [12] as follows. The initial product (50 g) was first dissolved in dry heptane (50 cm^3). Three aliquots of acetone (25 cm^3) were added to the mixture with ultrasonication between each addition. The solvent was then decanted and the precipitate of CaABS was rotary-evaporated to remove remaining solvent.

Table 1 Properties of polymer dispersants (*PD*) used in the experiments[a]

	DISPERSANT PD-I	DISPERSANT PD-II	DISPERSANT PD-III
Primary amine/ester ratio		1.4	
How received	45 wt% in 150 N oil		Pure (extracted)
Hydrodynamic radius R_H in heptane		16 nm	
How used	In 150 N oil, and in tetradecane	In iso-octane	In tetradecane

[a] PD-I is Exxon Paramins polymer no. 18808-3, PD-II is no. 18473-60-3, and PD-III is no. 17750-72-1

Solvents

The solvents were *n*-tetradecane, iso-octane and a mineral oil (150 N) which is branched alkanes (>97%) with an average of 22 carbons per molecule [12]. About 2–3% of the oil is *n*-alkanes and the remaining is branched alcohols (C_6–C_{11}).

Monolayer deposition

Monolayers of CaABS were deposited on mica surfaces at 20 °C at a surface pressure of 26 mN/m using the Langmuir–Blodgett technique [13, 14], resulting in a deposited area of 0.70 nm^2 per molecule (the monolayer collapses on water at the relatively low pressure of 34 mN/m).

Polymer solutions

The polymers were dissolved in three different oils: the mineral oil 150 N, *n*-tetradecane, and iso-octane. The polymer solutions were then centrifuged to remove particulates. The unperturbed hydrodynamic radius, R_H, of the functionalized polymer is estimated to be about 16 nm (result obtained from light-scattering measurements achieved by D.A. Weitz, unpublished results) although its Flory radius, R_F, could be higher or lower depending on the solvent conditions, which are not known for the solvents used in this study (see Table 1).

Force Measurements

The experiments were carried out using a SFA3. The general method and conditions have been well described in the literature [15, 16]. Experiments were done in either humid or humidity-free solution conditions. For the humidity-free experiments, a droplet of the liquid sample was injected between the two surfaces and dried overnight by placing a receptacle of P_2O_5 inside the sealed main chamber of the apparatus. Measurements commenced after the droplet had equilibrated with the dry vapor. For the dilution experiments, the main chamber was completely filled with the polymer solution without pre-drying the sample. All measurements were conducted at 25 °C. Interaction forces, F, normalized by the curvature radius of the surfaces, R, are plotted against surface separation, D, both linearly (A-type figures) and on semilog plots (B-type figures). Linear plots allow for an analysis of the adsorption and magnitude of the forces; semilog plots are more suitable for determining the maximum range of the forces and for comparing the measured force profiles with theory.

Thin-film viscosity measurements

Viscosity profiles (viscosity, η, as a function of gap thickness, D) were determined, using a modified SFA3, by the application of an a.c. voltage to the piezoelectric tube that supports the upper surface, causing it to vibrate at a known frequency v and amplitude A_o (Fig. 1). The viscous coupling of the liquid film between the two surfaces induces the lower surface to vibrate at the same frequency but with a reduced amplitude A and a nonzero phase ϕ relative to the upper surface. The solutions to the equations of motion for a system with a crossed-cylinder geometry and in the absence of any intermolecular force between the two surfaces (i.e., when the only opposition to flow is due to fluid viscosity) reduce to simple expressions at small separations ($D \ll R$) and amplitudes ($A \ll D$) [8, 9, 17]:

$$\eta(D) = \frac{KD}{12\pi^2 R^2 v\left[\left(\frac{A_0}{A}\right)^2 - 1\right]^{1/2}} \quad (\text{for } A \ll D)\ , \tag{1}$$

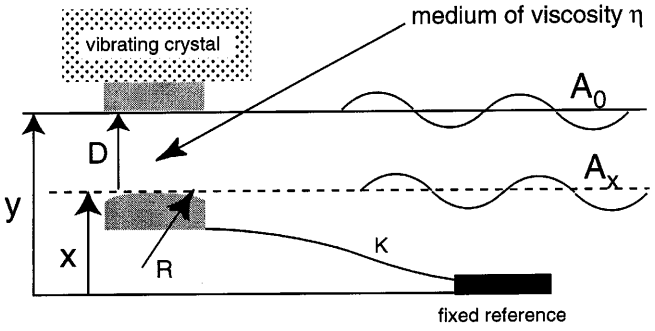

Fig. 1 Schematic representation of the experimental setup. The upper surface vibrates with driving amplitude A_0. Hydrodynamic (viscous) forces cause the lower surface to vibrate with different amplitude and phase so that the intersurface separation oscillates with amplitude A about a mean separation D [8]

where η is the average shear viscosity of the liquid in the gap, R is the curvature radius of the two surfaces, K is the stiffness of the normal force-measuring spring that supports the lower surface, and v is the driving frequency. For low shear rates ($v < 3$ Hz) the movement of the interference fringes can be monitored by a video camera and recorded for later analysis. Thus, all the relevant experimental parameters, D, A_o, A, K, R and v, are directly measurable. For a Newtonian liquid, a plot of $12\pi^2R^2v\,[(A_o/A)^2 - 1]^{1/2}/K$ versus D should yield a straight line of slope $1/\eta$ and intercept of $2\Delta_H$, where Δ_H is the distance of the shear plane from each surface, i.e., the hydrodynamic layer thickness per surface. Equation (1) is valid for low amplitudes and low frequencies, i.e., low shear rates, where inertial and acceleration terms can be ignored and the only opposition to flow is due to fluid viscosity.

Dynamic Light Scattering

To determine the interactions of the new dispersants with colloidal particles, the dispersant samples were mixed with a suspension of magnesium carbonate colloidal particles (similar to the colloidal particles used in lubricants) coated with CaABS surfactant. DLS measurements were performed to determine the size of the colloidal particles. Adsorption of the dispersant molecules on the surfaces of the colloidal particles should increase their hydrodynamic radius, and this should be measurable with DLS. The PD samples were mixed with a suspension containing about 50% by weight of colloids, and stirred at about 70 °C for several hours to assure full adsorption. For the DLS measurements, the mixture was diluted by a factor of about 15 in heptane. This reduced the optical absorption of the sample to an acceptable level, although thermal lensing of the laser beam was still observed, necessitating the use of very low input powers for the measurements. The heptane also ensured that the solvent viscosity was low, improving the quality of the data. The samples were filtered and centrifuged gently to remove any dust particles from the beam; nevertheless, great care still had to be taken to ensure that the data were not distorted by dust or other larger particles.

The DLS was performed in a standard goniometer, allowing measurements to be performed at different scattering angles. This proved convenient to assist in identifying the deleterious effects of any remnant dust. Once this was accomplished, the data were independent of scattering angle, as expected. The data were analyzed using standard cumulant methods to obtain the hydrodynamic radii of the colloidal particles which are reported here. The particles were reasonably monodisperse, as determined from the value of the second cumulant. This allowed us to measure their

size with sufficient accuracy to determine the changes in their hydrodynamic radii upon adsorption of the surfactant molecules.

Bulk-viscosity measurements

The kinematic viscosity of the concentrated colloidal dispersions were measured using a capillary tube. All measurements were performed in a thermostatted bath at 100 °C.

Results and discussion

Forces between bare mica surfaces with and without polymer

As a control, the forces between two mica surfaces across pure 150 N oil (without polymer) were measured first. As shown in Fig. 2A, these short-range forces were similar to those previously measured in other hydrocarbon liquid mixtures [12], exhibiting a weak attraction (not shown in Fig. 2A) at $D \approx 2.0$–2.5 nm and a steep steric "hard-wall" repulsion at $D \approx 1.5$ nm, corresponding to a few compressed hydrocarbon chains.

Addition of PD-I to the oil caused a distinct layer to adsorb, pushing out the "hard wall" to $D = 11$ nm, which corresponds to a compressed polymer layer 5.5 nm thick on each surface. The polymer probably adsorbs via the binding of its amino groups to the mica surfaces. The resulting "equilibrium" force curves were repulsive at all separations as shown in Fig. 2A (linear plots) and B (semilog plots). Equilibrium here means that the forces were reversible and unchanged over the time period of a force run, which typically lasts about 1 h. The true equilibrium interaction could very well be different, even attractive.

Figure 2B shows that the forces display the typical S-shaped profile (on a semilog plot) characteristic of the "steric" forces between adsorbed polymer layers (mushrooms, brushes, etc.) [4, 18–23]. Their range of 65–100 nm implies an expanded layer of thickness 33–50 nm per surface. This is 2–3 R_H per surface which is indicative of significant tail contributions to the interaction.

The asymptotic "tail-ends" of the measured force curves were unexpectedly variable from run to run, and no systematic reason for these variations could be found (but see discussion later). We should note, however, that these variations generally occurred at distances D greater than 25 nm, where the forces are already quite weak. For two colloidal spheres of radii $R = 7$ nm (see light scattering results later) these tail-end contributions (at $D > 3\ R_H$) to the total interaction energy would be less than the thermal energy.

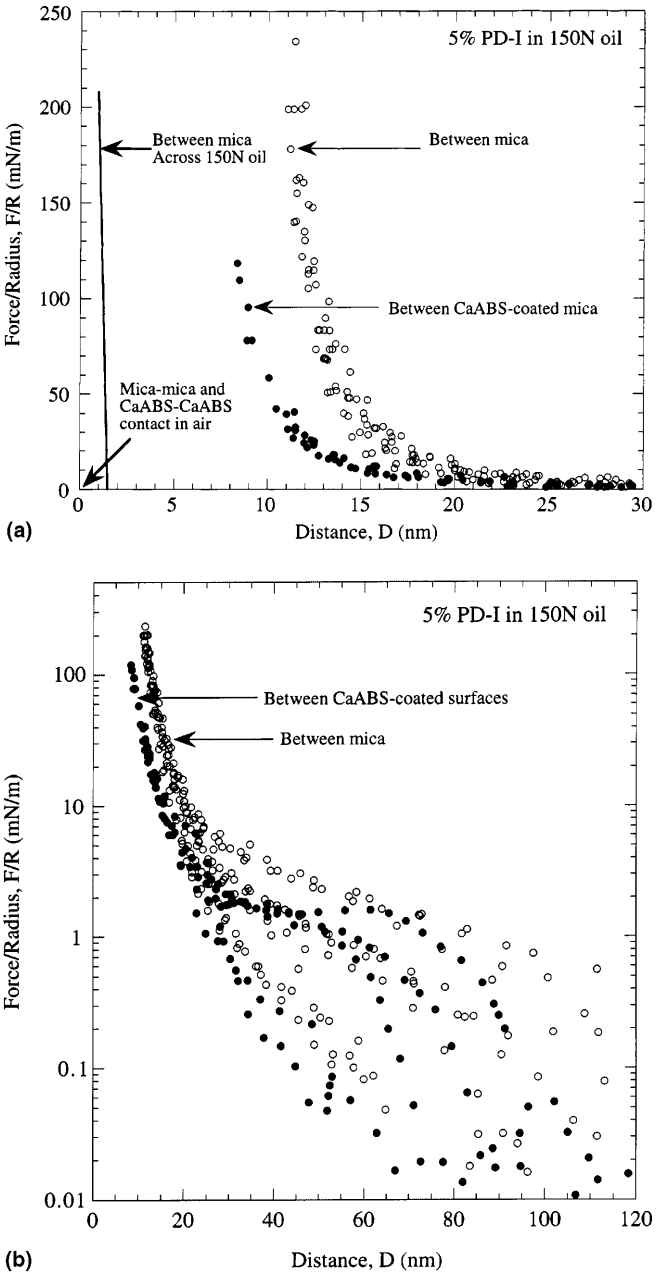

Fig. 2 **A** Measured forces between mica (○) and calcium alkylbenzene sulfonate (*CaABS*)-coated mica (●) surfaces in dry 150 N oil with no added polymer (—) and with 5% polymer dispersant (*PD*)-I at 25 °C. Contact ($D = 0$) is here defined as the positions of the mica or surfactant-coated mica surfaces in adhesive contact in air before addition of fluid to the measuring chamber. The CaABS surfaces have a 1.5–2.0 nm-thick monolayer deposited on each surface, so that at "contact" ($D = 0$) the mica surfaces are actually 3–4 nm away from each other. The inward shift (~3.5 nm) of the force curves across the CaABS surfaces shows that the surfactant layers were displaced by the polymer (or that less polymer adsorbs to these surfaces). **B** Logarithmic plot of data of in **A**, showing the large variation (scatter) in the tail-end low-force regions of the measured forces, but not in the short-range regime (this is the reason for the apparent absence of scatter in the linear plots of **A**)

Forces between surfactant-coated mica surfaces

The forces between mica surfaces were then compared to the forces between CaABS-coated mica surfaces immersed in the same PD-I solution. The resulting force profiles are also shown in Fig. 2A and B. They are very similar to those measured between two bare mica surfaces, only shifted inwards by 3.5 nm – almost exactly the thickness of two CaABS monolayers [12]. Note that in this experiment the reference $D = 0$ corresponds to the contact of the two CaABS surfaces in air. The thicknesses of the CaABS monolayers were measured in air by comparing the contact positions before and after the depositions. In this way a value of 1.4 nm per monolayer (in air) was obtained. These results therefore suggest that the polymer displaces the CaABS monolayer to adsorb on the mica surface since the magnitude, range and profile of the forces are essentially identical when referred to the bare mica surfaces (cf. the two sets of curves in Fig. 2A, B).

Effect of polymer concentration and solvent type

Figure 3 shows the difference between the 5% and 0.5% samples of PD-I under the same conditions as in Fig. 2. In the more concentrated solution, the position of the hard-wall is 3 nm farther out (at $D = 11$ nm compared to $D = 8$ nm), which is indicative of greater adsorption; however, the force profiles are very similar. Indeed, an order of magnitude difference in the bulk polymer concentration causes only a moderate change in the overall force, indicating that at 0.5% the adsorption is already approaching the saturation value.

The results of experiments with PD-II polymer in iso-octane at concentrations of 5, 7 and 12% are shown in Fig. 4. The magnitude and range of the forces between the mica surfaces are very similar to those for PD-I in 150 N oil shown in Fig. 3. The results with this polymer also showed a small effect of concentration although here the concentration was varied by a factor of only 2.4.

The experiments described previously (Figs. 2–4) were "droplet" experiments, where each sample was prepared separately and each force curve represents a different experiment. Thus, there was no gradual increase or decrease in the polymer concentration in these experiments. Such droplet experiments are convenient when very high polymer concentrations are being studied and/or where totally dry conditions are required.

For the following experiments, the whole apparatus chamber was filled with the polymer solution. In this way, it was possible to study the effect of gradually increasing or decreasing the concentration by concentrating or diluting the solution. Unlike the droplet samples described earlier these bulk samples are difficult

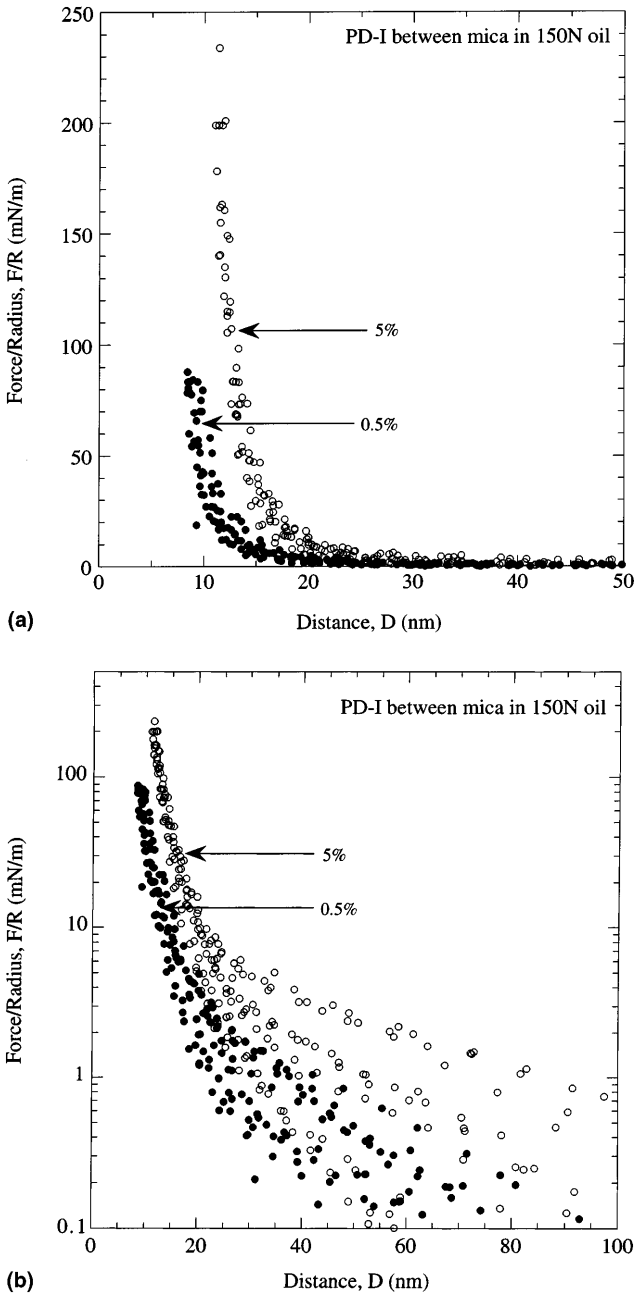

Fig. 3 **A** Forces between mica surfaces across 5% (○) and 0.5% (●) PD-I in 150 N oil. Each concentration corresponds to a different experiment with a freshly prepared solution. **B** Same data as in **A**, but plotted on a logarithmic scale. Again, one may note the large variations (scatter) in the tail ends of the forces, but not in the short-range regime

to dry and so were used "as is"; however, the effect of drying the sample was not significant.

The results of experiments with PD-III (which is equivalent to PD-II without synthesis oil) in *n*-tetradecane are shown in Figs. 5–7. First, the forces across bare mica (Fig. 5) are of slightly longer range and decay more

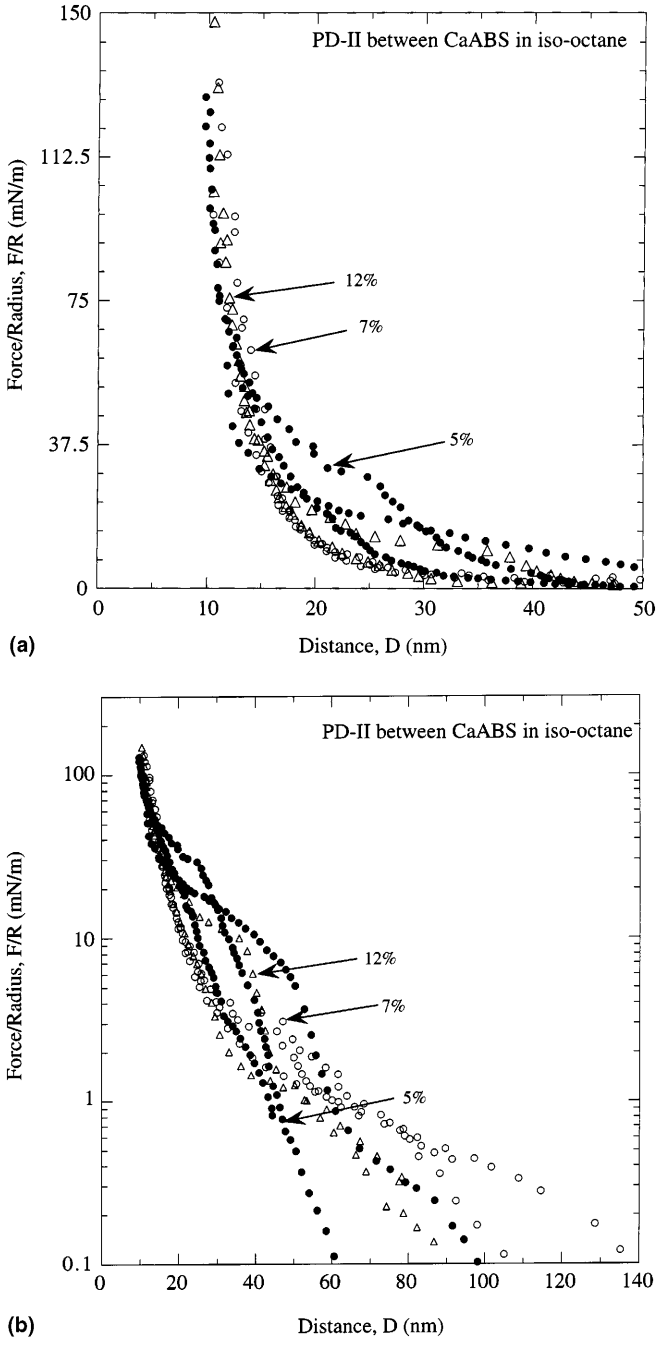

Fig. 4 **A** Forces between CaABS-coated mica surfaces across different concentrations of PD-II in iso-octane, (●): 5%, (○):7%, (△): 12%. Note, however, that since the original PD-II polymer contained a roughly equal amount of 150 N oil (see Table 1) the dispersing media were not pure iso-octane but contained 5–12% of 150 N oil. In these experiments, each sample was separately prepared for each experiment. **B** Same data as in **A**, but plotted on a logarithmic scale

steeply than the forces shown in Figs. 2 and 3 when compared at similar concentrations. This shows that different hydrocarbon solvents may have a small but significant effect on the adsorption and on the range and magnitude of colloidal interactions mediated by these polymers. Tetradecane appears to cause more adsorption (larger hard-wall thickness) and a shorter-range (more steeply decaying) repulsive force, both of which are consistent with a reduced solvent quality compared to iso-octane and 150 N oil. Also significant was the finding that after rediluting the 8% solution to 0.01% the force profile was unchanged (cf. ○ and △ points in Fig. 5), which is indicative of strong, irreversible adsorption.

The forces measured between CaABS-coated mica surfaces in tetradecane with the pure PD-III polymer at different concentrations are shown in Fig. 6. A comparison of the forces between mica (Fig. 5) and between CaABS (Fig. 6) in the 1% PD-III solutions is given in Fig. 7. As was found for PD-I in 150 N oil (cf. Fig. 2), the inward shift (~4 nm) of the forces between CaABS confirm that this polymer also displaces the surfactant monolayer; however, the amount of polymer adsorbed appears to be slightly less than on mica (cf. Fig. 7A), less sensitive to concentration, and partially reversible, indicating that competition with the surfactant is always present, i.e., that the displaced surfactant probably remains associated with the polymer layer.

It can be mentioned that the presence of small amounts of water and octanol introduced into the polymer solutions from the vapor phase did not show any significant effect on the forces. However, controlled experiments at different polar solute activities were not conducted.

Viscous forces

As described in the Experimental section and as defined by Eq. (1), if the data points, corresponding to the values of $12\pi^2R^2v\,[(A_o/A)^2 - 1]^{1/2}/K$, at all separations fall on a straight line that extrapolates back to pass through the origin at $D = 0$, the film viscosity is constant and equal to the bulk value, and the nonslip plane is located at the solid–film interface. This is the "ideal" situation. When the line is straight but does not pass through the origin, the far-field points fall on the straight line that usually has a slope corresponding to the bulk viscosity. In addition, the intercept of that line with the distance axis at $D = D_o$ gives twice the hydrodynamic layer thickness Δ_H according to $D_o = 2\Delta_H$.

Viscous forces were measured between mica and surfactant-coated surfaces across films of PD-III in tetradecane and the results are shown in Fig. 8. The measured far-field viscosities correspond to the bulk viscosity since all data points fall on a straight line. The inverse slope of the line gives the viscosities (given in Table 2) which, after a statistical analysis of the points, gives an error of ± 0.002 *P*. This error corresponds to

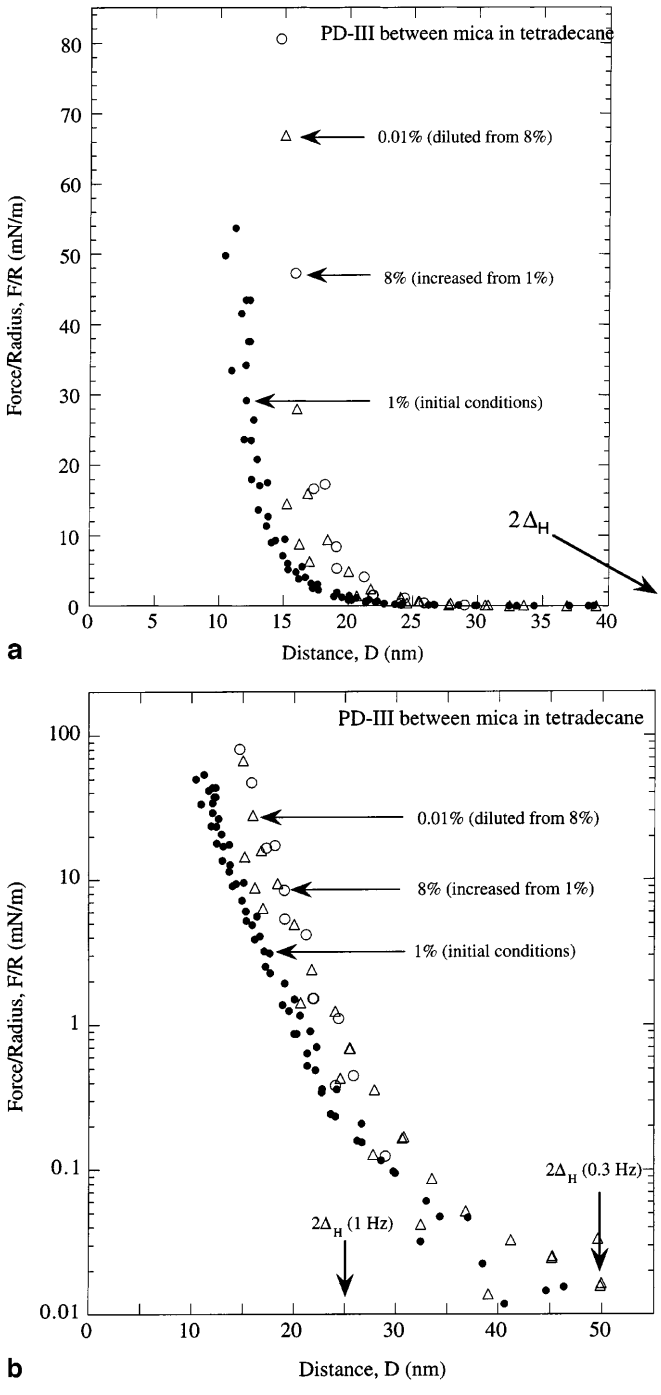

Fig. 5 **A** Forces between mica surfaces across different concentrations of polymer PD-III in tetradecane, (●): 1% (initial conditions), (○): 8% (increased from 1%), (△): 0.01% (diluted from 8%). Force measurements at each new concentration commenced after 1 day of equilibration and continued for about 2 days. Final "hard-wall" positions following high compression ($F/R \sim 100$ mN/m) are at 11 and 15 nm for 1% and 8%, respectively. **B** Same data as in **A**, but plotted on a logarithmic scale. Also shown by *arrows* are the separations corresponding to the effective planes of slip for the two surfaces, as deduced from the far-field viscosity runs of Figs. 8 and 9

the random error arising from the scatter in the experimental points. It has to be noted that the bulk viscosity values obtained with the SFA were close to the measured viscosity obtained using a capillary tube (J.P Stokes, unpublished results). The error in the measured value of the viscosity η comes mainly from the systematic error in measuring the radius R (which can lead to an error of 10–15% in the measured viscosity) [9]. It has previously been shown that the data of viscous-force measurements between two bare (uncoated) mica surfaces across pure tetradecane lead to a straight line extrapolating through the origin yielding $\Delta_H \approx 0$ [9]. Returning to Fig. 8, in the polymer solutions, the finite intercepts at $D_0 \approx 52$ nm (see Table 2) are indicative of adsorbed polymer layers of hydrodynamic thickness $\Delta_H \approx 26$ nm per surface (about 1.5 R_H). The locations of the slipping planes at Δ_H do not vary significantly with bulk polymer concentration, in agreement with the force measurements of Fig. 5; that is, they depend on the amount of polymer adsorbed at the time of the measurements even if this adsorption may not be the equilibrium adsorption but some metastable "restricted equilibrium" or "irreversible" adsorption. Most importantly, the far-field data show that the polymer tails, even when they contribute negligibly to the interaction forces, dominate the mean gap viscosity by effectively determining the hydrodynamic layer thickness, Δ_H. These values, given in Table 2, are indicated on Fig. 5. These somewhat large values imply that the effective viscosity of a colloidal dispersion is expected to increase above the bulk value (the value for the pure solvent in the absence of polymer) once the film thickness falls below $2\Delta_H$. This, however, is not necessarily the same as the separation at which the viscosity "shoots up", this might occur at much smaller separations, closer to the "hard walls" in the force measurements, and depends on the detailed way the near-field data points curve away from the far-field line. We may thus distinguish between a far-field and near-field value for Δ_H which, as shown later, also appear to depend on the shear rate.

The effects of driving frequency (shear rate) on the viscous forces is shown in Fig. 9. At all polymer concentrations, increasing the driving frequency from 0.3 to 1 Hz results in a significant reduction – by as much as 50% – of the far-field hydrodynamic layer thickness. This is indicative of unusual large shear-alignment effects of the outermost tail regions of the adsorbed layers, which is also consistent with the variability seen in the far-field forces.

Similar viscosity measurements were done with PD-III in tetradecane between CaABS-coated mica surfaces, and slightly different results were obtained, as illustrated in Fig. 10. The far-field hydrodynamic layer thickness values are lower than for adsorption on mica, viz., $\Delta_H = 9.5$ nm compared to $\Delta_H = 26$ nm at 0.3 Hz for the 8.2% solution, which is also consistent with the

lower adsorption of CaABS deduced from the force measurements. Beyond the shear planes, the viscosities of the polymer solutions again exhibited their bulk shear viscosities. The effect of frequency (shear rate) was less dramatic than was observed between mica and, in this case, an increase in frequency gave rise to an increased hydrodynamic layer thickness. These viscosity results also show that while polymer replaces or penetrates the CaABS monolayers, the surfactant remains associated with the polymer because it has an effect on the dynamic interactions, again consistent with the static force measurements. However, more detailed measurements would need to be done, both at smaller separations and over a much larger range of frequencies, to fully characterize the thin-film rheology of this complex system.

Light-scattering results

The hydrodynamic radius of the colloidal particles determined by DLS was 7 nm. This represents the size of the magnesium particle ($MgCO_3$) plus its surfactant coating (CaABS). The measured size is consistent with independent results obtained from small-angle neutron-scattering measurements [M.Y. Lin, J.S. Stokes, unpublished results]. Upon mixing with the PD, the measured hydrodynamic radii of the particles increased, confirming the adsorption of the dispersant on the particle surfaces. Moreover, the increase in radius was directly proportional to the degree of polymerization, as shown in Fig. 11; the radii of gyration, and hence the hydrodynamic radii, of the dispersants are expected to increase as the degree of polymerization is increased. These results are consistent with the SFA measurements in that the size of the PDs as determined by the increase in the hydrodynamic radii of the colloids, corresponds reasonably well with the size of the molecules as determined by the separation where forces are measured with the SFA. For example, large, reproducible forces are measured for PD-I at separations between 20 and 30 nm (10 and 15 on each surface); by comparison, the smallest dispersant studied with DLS increased the hydrodynamic radius of the colloidal particles by about 12 nm (7–19 nm), in close correspondence with the SFA separation. This comparison confirms that the conclusions from the surface force measurements are directly relevant to our understanding of the stability of the colloidal particles. They show that the adsorption of the dispersant can indeed provide steric stabilization for the colloidal particles; moreover, the DLS results suggest that an increase in the degree of polymerization of the PD also corresponds directly to an increase in the range of this steric interaction, which should further increase the stability of the colloidal particles.

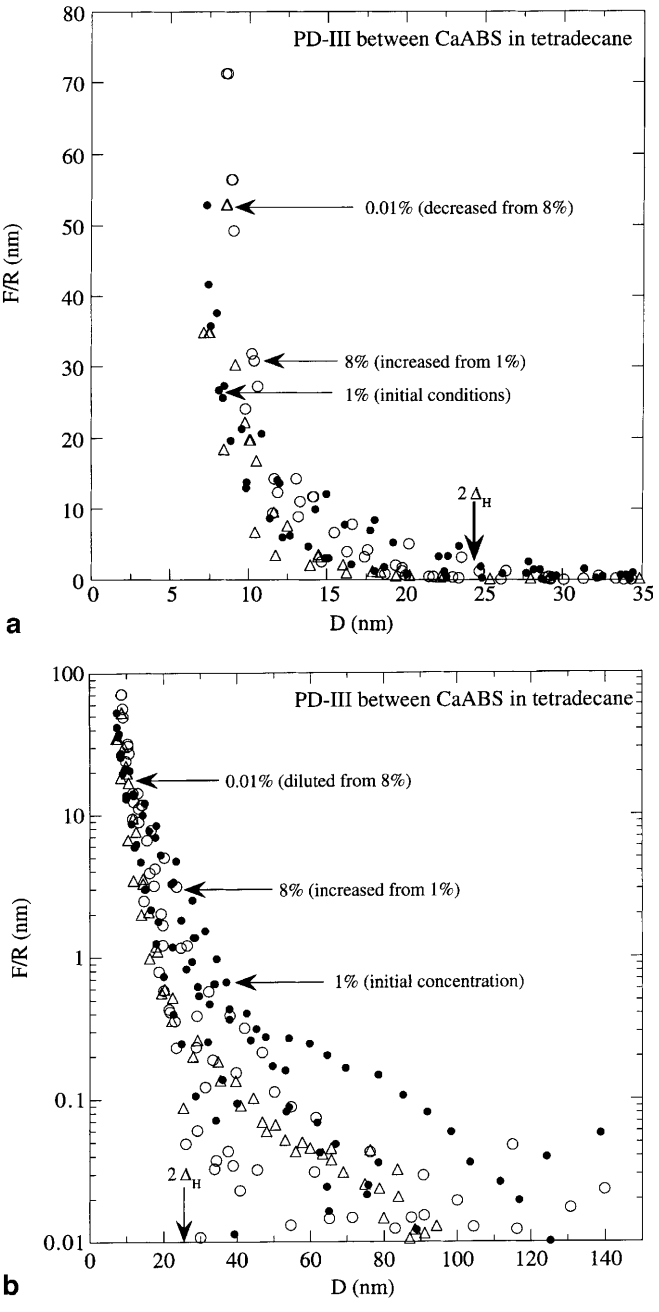

Fig. 6 **A** Forces between CaABS-coated mica surfaces across different concentrations of PD-III in tetradecane, (●): 1% (initial conditions), (○): 8% (increased from 1%), (△): 0.01% (diluted from 8%). Force measurements at each new concentration commenced after 1 day of equilibration and continued for about 2 days. The scatter in the data reflects the variations in the force runs obtained over this time period. *Vertical arrows* show the separations corresponding to the effective plane of slip for the two surfaces, as deduced from the far-field viscosity runs of Fig. 9. Note the decreased range of both the forces and the hydrodynamic layer thickness, Δ_H, compared to those between bare (uncoated) mica surfaces. **B** Same data as in **A**, but plotted on a logarithmic scale. Note the greater reversibility of the force on dilution than occurred with bare mica surfaces

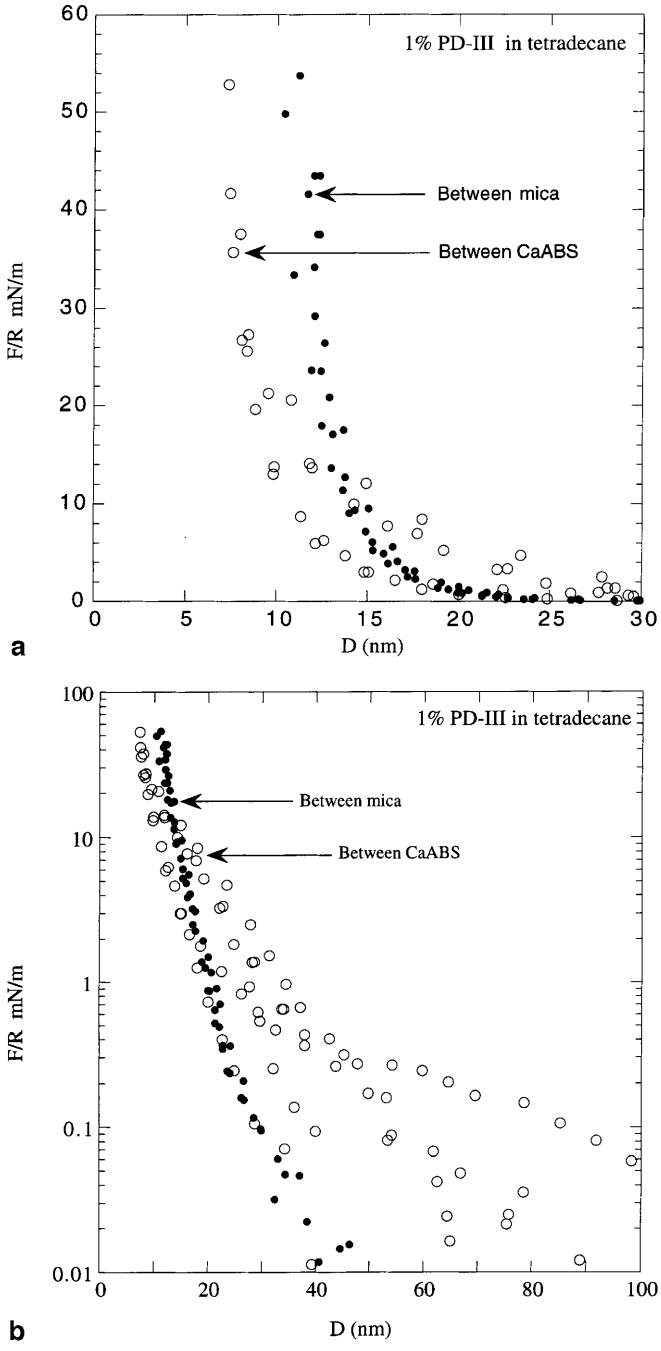

Fig. 7 **A** Comparison of the forces between mica (●) and CaABS-coated (○) mica surfaces across 1% PD-III in tetradecane. Final 'hard-wall' positions following high compression ($F/R \sim 100$ mN/m) are indicated by the *vertical arrows* at 11 and 7 nm for mica and CaABS, respectively. The inwards shift (~4 nm) of the force curves across the CaABS surfaces shows that for this system the surfactant layers were also displaced by the polymer (cf. Fig. 2). **B** Same data as in **A**, but plotted on a logarithmic scale

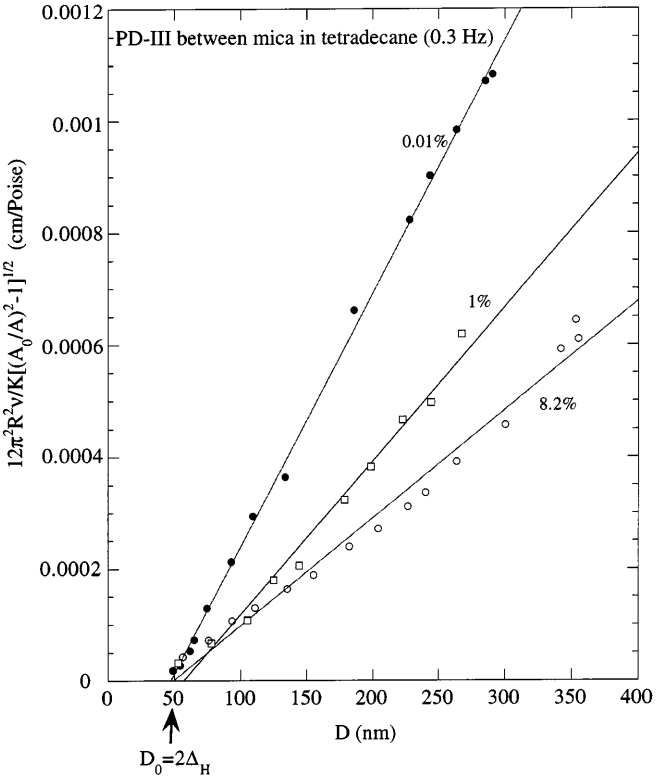

Fig. 8 Plot of $12\pi^2R^2v\,[(A_o/A)^2 - 1]^{1/2}/K$ versus surface separation D for two mica surfaces at different concentrations of PD-III in tetradecane at $v = 0.3$ Hz and $T = 25$ °C. (●): 0.01%, (□): 1%, (○):8.2%. The inverse slope of each curve corresponds to the shear viscosity of the fluid in the gap. The intercept on the D-axis corresponds to $2\Delta_H$ where Δ_H is the far-field hydrodynamic layer thickness per surface

Further support for this behavior comes from the viscosity measurements of the colloidal particles with the adsorbed dispersant molecules. At low concentrations, the viscosity increased by only a small amount, and approximately linearly, with increasing colloid concentration. However, as the concentration increased further, the viscosity diverged sharply, reflecting strong interactions between the colloidal particles as their effective volume fraction increased. The onset of this divergence must reflect the concentration where the effective volume fraction of the colloidal particles approaches close packing. This onset varied significantly with the degree of polymerization of the adsorbed dispersant. For the shortest dispersant used, the onset occurred at a concentration of about 0.3 wt%. We note that the density of the colloid core is about 2 gm/cm^3, so the effective volume fraction of colloidal particles themselves is less than 0.15. Thus, this divergence reflects an increased effective volume fraction of the particles due to the coating of the dispersant. As the length of the dispersant molecules increased, the concentration of the viscosity divergence decreased, and so, for the largest dispersant, the divergence occurred at a concentration of about 0.02 wt%. This reflects the great increase in the effective size of the

Table 2 Experimental results of the thin-film vicosity measurements with PD-III at different concentrations in tetradecane

Concentration (weight %)	Surfaces	Driving frequency (Hz)	Viscosity (η) (cP)	Hydrodynamic layer thickness (Δ_H) (nm)
0.01	Mica	0.3	2.2	23.5
0.01	Mica	1.0	2.4	13.5
1	Mica	0.3	3.6	28.5
1	CaABS-coated mica	0.3	3.6	10.5
1	CaABS-coated mica	1	3.7	16.0
8.2	Mica	0.3	5.2	26
8.2	Mica	1.0	6.5	10.5
8.2	CaABS-coated mica	0.3	6.6	9.5
8.2	CaABS-coated mica	1.0	6.5	22.5

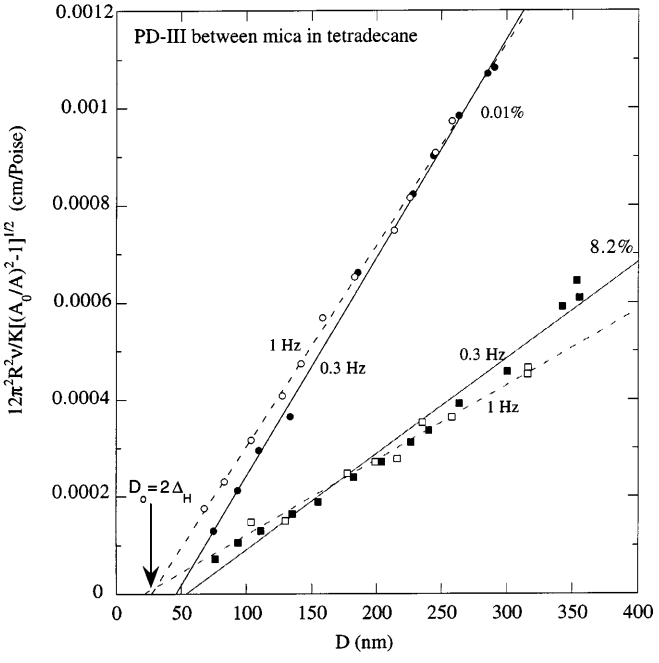

Fig. 9 Plot of $12\pi^2R^2v\ [(A_o/A)^2 - 1]^{1/2}/K$ versus surface separation D for two mica surfaces at two different concentrations of polymer PD-III in tetradecane, measured at two different frequencies of $v = 0.3$ Hz and $v = 1$ Hz. (○):0.01%, 1 Hz, (●):0.01%, 0.3 Hz, (□): 8.2%, 1 Hz, (■): 8.2%, 0.3 Hz

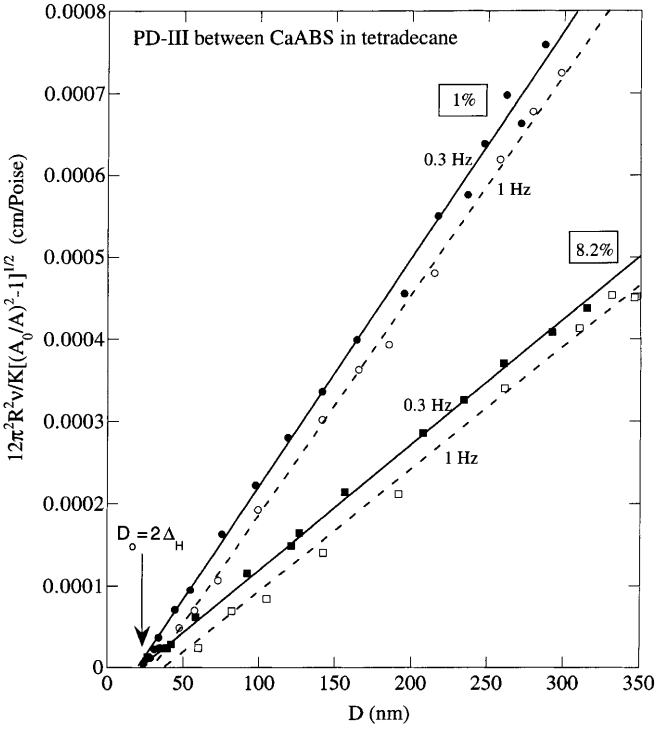

Fig. 10 Plot of $12\pi^2R^2v\ [(A_o/A)^2 - 1]^{1/2}/K$ versus surface separation D for two CaABS-coated mica surfaces at different concentrations of PD-III in tetradecane, measured at $v = 0.3$ Hz and $v = 1$ Hz. (○):0.01%, 1 Hz, (●):0.01%, 0.3 Hz, (□): 8.2%, 1 Hz, (■): 8.2%, 0.3 Hz

colloidal particles as the length of the adsorbed dispersant increases.

Conclusions

The static and dynamic forces between adsorbed layers of functionalized polymer in various hydrocarbon solvents displayed some very complex time- and history-dependent interactions. In spite of this complexity, however, the interactions were qualitatively very similar even though three different polymers, three solvents and two different surfaces were studied. Our main conclusions are summarized under the following three properties.

1. Adsorption. The polymer adsorbs via its amino groups on bare mica surfaces and to CaABS-coated mica surfaces by displacing or penetrating through the physisorbed CaABS monolayer. Presumably, to avoid such displacement effects, surfactant monolayers would have to be chemically grafted or chemisorbed to surfaces. The adsorption is already near to saturation at 0.1% bulk polymer concentration, but continues to increase even at 8%. The adsorption appears to be "irreversible" over time scales of a few days. The adsorption also depends on the solvent, differing

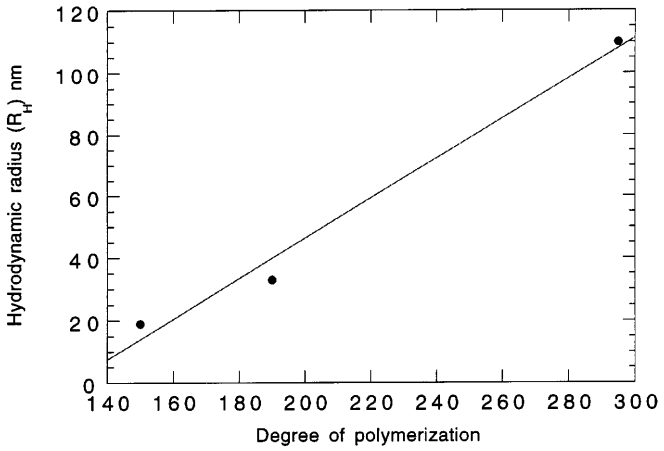

Fig. 11 Variation of the hydrodynamic radius as a function of the degree of polymerization of the polymer dispersant molecule

between different solvents even when they are good solvents.

2. Colloidal forces. The static interactions are monotonically repulsive at all separations. The far-field (long-range) forces are characteristic of polymer-like steric forces, and have a range of 60–100 nm, which is significantly greater than the hydrodynamic radius of the polymer. However, a brush-type adsorption appears to be unlikely. Perhaps the adsorbed polymer agglomerates or entangles with "free" polymer to extend the effective range of the interaction; however, the most likely reason is that the tails play a more significant role than with higher-molecular-weight polymers. The forces are quite sensitive to the nature of the solvent, both through its effect on the adsorption (which determines the magnitude of the forces) and its effect on the coil size R_H (which determines the range of the forces); however, water and other small polar solutes such as octanol do not appear to have an effect on the far-field forces.

3. Viscous properties. The far-field rheological properties can be accounted for in terms of an immobilized layer per surface having a (hydrodynamic) layer thickness Δ_H of about 26 nm on bare mica, and 10 nm on CaABS-coated mica at a driving frequency of 0.3 Hz. Beyond Δ_H per surface, or $2\Delta_H$ for two surfaces, the viscosity is the same as that of the bulk polymer solution. However, both shear-thinning and shear-thickening effects were observed which show that the values of Δ_H are shear-rate dependent, reflecting the sensitivity of the outermost tail regions of the adsorbed layers to flow even at low shear rates ($<10^2$ s^{-1}). These observations may explain the great variability observed in the asymptotic tail regions of the force curves: if the polymer tail conformations are highly sensitive to shear, then the far-field forces would also be expected to be dependent on the rate of approach of the two surfaces during the force measurements or even to the previous history.

These observations therefore suggest that concentrated colloidal dispersions containing functionally adsorbed polymers may exhibit forces and rheological properties that could be very sensitive to shear rate. The complete spectrum may well be a complex one and a complete understanding would require a detailed study to be made of the WLF (Williams, Landel, Flory) parameters [24] that describe both the bulk and thin-film rheological behavior of the dispersions.

Acknowledgments This work was supported by Exxon Chemical Company, Linden, New Jersey, and Exxon Corporate Research & Engineering Laboratory, Clinton, New Jersey. The light-scattering measurements were performed by A.H. Krall and D.A. Weitz at Exxon Research and Engineering, and the kinematic viscosity data were provided by J.P. Stokes at Exxon Chemical Company.

References

1. Cracknell R (1993) Lubr Eng 49:129–135
2. Balazs AC, Huang K, Pan T (1993) Colloids Surf A 75:1–20
3. Patel S, Tirrell M (1989) Annu Rev Phys Chem 40:597
4. Israelachvili JN (1992) Intermolecular and surface forces, 2nd edn. Academic Press, London
5. Kuhl TL, Guo Y, Aldferfer JL, Berman A, Leckband D, Israelachvili JN, Hui SW (1996) Langmuir 12:3003–3014
6. Ruths M, Yoshizawa H, Fetters L, Israelachvili JN (1996) Macromolecules 29:7193–7203
7. Klein J, Kamiyama Y, Yoshizawa H, Israelachvili JN, Fredrickson GH, Pincus P, Fetters LJ (1993) Macromolecules 26:5552–5560
8. Israelachvili JN (1986) J Colloid Interface Sci 110:263–271
9. Israelachvili JN (1986) Colloid Polym Sci 264:1060–1065
10. Horn RG, Israelachvili JN (1988) Macromolecules 21:2836–2841
11. Gee ML, Tong P, Israelachvili JN, Witten TA (1990) J Chem Phys 93:6057–6064
12. Gee ML, Israelachvili JN (1990) J Chem Soc Faraday Trans l 86:4049–4058
13. Marra J (1985) J Colloid Interface Sci 107:446–458
14. Marra J (1986) J Colloid Interface Sci 108:11–22
15. Israelachvili JN, McGuiggan PM (1990) J Mater Res 5:2223–2231
16. Israelachvili JN, Adams GE (1978) J Chem Soc Faraday Trans I 74:975–1001
17. Horn RG (1989) Chem Phys Lett 162:404–411
18. Dolan A, Edwards F (1974) Proc R Soc Lond Ser A 337:509–516
19. Alexander S (1977) J Phys (Paris) 38:983–987
20. de Gennes P (1981) Macromolecules 14:1637–1644
21. de Gennes P (1987) Adv Colloid Interface Sci 27:189–209
22. Milner S, Witten T, Cates M (1988) Macromolecules 21:2610–2619
23. Murat M, Grest GS (1989) Macromolecules 22:4054–4059
24. Ferry JD (1980) Viscoelastic properties of polymers, Wiley, New York